Galvin, R. and Gurevich, B. 2015. Frequency-dependent anisotropy of porous rocks with aligned fractures. Geophysical Prospecting. 63 (1): pp. 141-150.

Frequency dependent anisotropy of porous rocks with aligned fractures

Robert J. Galvin[1] *and Boris Gurevich*[2]

ABSTRACT

Naturally fractured reservoirs are becoming increasingly important for oil and gas exploration in many areas of the World. Because fractures may control the permeability of a reservoir it is important to be able to find and characterise fractured zones. In fractured reservoirs, the wave induced fluid flow between pores and fractures can cause significant dispersion and attenuation of seismic waves. For waves propagating normal to the fractures this effect has been quantified in earlier studies. Here we extend normal incidence results to oblique incidence using known expressions for the stiffness tensors in the low- and high-frequency limits. This allows us to quantify frequency-dependent anisotropy due to the wave-induced flow between pores and fractures and gives a simple recipe for computing phase velocities and attenuation factors of quasi-P and SV waves as functions of frequency and angle. These frequency and angle dependencies are concisely expressed through dimensionless velocity anisotropy and attenuation anisotropy parameters. It is found that while at low frequencies the medium is close to elliptical (which is to be expected as a dry medium containing a distribution of penny-shaped cracks is known to be close to elliptical), at high frequencies the coupling between P and SV waves results in anisotropy due to the non-vanishing excess tangential compliance.

INTRODUCTION

Naturally fractured reservoirs are becoming increasingly important for oil and gas exploration in many areas of the World. Because fractures may control the permeability of a reservoir it is important to be able to find and characterise fractured zones. In order to

characterise a fractured reservoir we need to understand the effect the fractures will have on its overall elastic properties. Fractures are highly compliant compared to the relatively stiff pores, so fluid will flow between pores and fractures during passage of the seismic wave. If the fractures are aligned, the reservoir will exhibit long wavelength effective anisotropy. Since the fluid flow and scattering taking place due to the fractures depends upon seismic frequency, the anisotropy will be frequency-dependent.

In the limit of low frequencies, static models can be used to obtain the effective elastic moduli of the fluid-saturated medium in terms of the properties of the dry skeleton and the saturating fluid (Gassmann (1951); Brown and Korringa (1975); Thomsen (1995); Gurevich (2003); Cardona (2002)). For these models to be valid, fluid pressure must have time to fully equilibrate throughout the connected pore space which will only be the case at low frequencies. At higher frequencies pressure equlibration will be incomplete causing frequency dependent and anisotropic attenuation and dispersion. Anisotropic attenuation and dispersion have attracted considerable interest in recent years (Behura and Tsvankin (2009); Best, Sothcott and McCann (2007); Carcione, Santos and Picotti (2012); Carcione, Picotti and Santos (2012); Chichinina, Obolentseva and Ronquillo-Jarillo (2009); Chichinina, Obolentseva, Gik, Bobrov and Ronquillo-Jarillo (2009); Clark, Benson, Carter and Guerrero-Moreno (2009); Wenzlau, Altmann and Muller (2010); Zhu, Tsvankin, Dewangan and van Wijk (2007)). Analysis of these effects for a porous and fractured medium requires a dynamic model of interaction of an elastic wave with an ensemble of fractures in a porous medium.

A number of schemes tackling this dynamic problem in fractured porous rocks are currently available. Brajanovski, Gurevich and Schoenberg (2005) model a fractured medium as very thin, highly porous layers in a porous background. Their model implies that these fractures are of infinite extent and therefore is valid when fracture spacing is much smaller than fracture length (diameter). The case of finite-size fractures was considered by Hudson, Liu and Crampin (1996), who model fractures as thin penny-shaped voids, and account for fluid flow effects by applying the diffusion equation to a single crack and ignoring interaction between cracks. This approximation however leads to some unphysical effects, such as

the result that the anisotropy of the fluid-saturated fractured and porous rock in the low frequency limit is the same as for the dry rock (Hudson, Pointer and Liu (2001); Chapman (2003); Brown and Gurevich (2004)). Chapman (2003) and Maultzsch et al. (2003) analyze frequency-dependent anisotropy caused by the presence of mesoscale fractures in a porous rock, by considering connectivity of individual fractures, pores and microcracks. A more general computational model which can take account of pores and fractures of any size and shape was proposed by Jakobsen, Johansen and McCann (2003) using the T-matrix approximation, commonly used to study effective properties of heterogeneous media. In the T-matrix approximation the effect of voids (pores, fractures) is introduced as a perturbation of the solution for the elastic background medium.

Galvin and Gurevich (2009) modeled the effect of fractures as a perturbation with respect to an isotropic porous background medium. This approach was attractive because it allowed us to use all the machinery of the theory of wave propagation in fluid-saturated porous media, known as the theory of poroelasticity (Biot, 1962), without specifying individual shapes of grains or pores. It is also logical to assume that the perturbation of the porous medium caused by the introduction of fractures will be much smaller than the perturbation caused by putting all the pores and fractures into an elastic solid.

Galvin and Gurevich (2009) simulated the effect of fractures by considering them to be thin circular cracks in a poroelastic background. They assumed that the cracks are mesoscopic (large compared to the pore size, but small compared to the fast wave wavelength). Using the solution of the scattering problem for a single crack (Galvin and Gurevich, 2007) and the multiple-scattering theory of Waterman and Truell (1961) they estimated the attenuation and dispersion of elastic waves taking place in a porous medium containing a sparse distribution of such cracks (Figure 1).

However the previous work was limited to normal crack incidence, and therefore only gives the effective properties in the direction normal to the cracks. In order to look at the anisotropy of the effective medium the scattering problem needs to be generalised to oblique angles of incidence, a problem currently being investigated. Carcione et al. (2013) study angular and frequency dependent properties of a fractured porous medium by obtaining

the five complex frequency dependent stiffnesses of the equivalent transversely isotropic (TI) medium. In this paper we present a simple approximate method for obtaining the complete effective stiffness tensor of a fluid-saturated porous medium with aligned cracks and investigate the predicted anisotropy behaviour. The entire analysis is restricted to the long wavelength limit so that the fracture size and spacing are assumed small compared to the wavelength (the so-called equivalent medium approximation).

BACKGROUND THEORY

Stiffness tensor of a dry fractured medium

The dry rock is assumed to be a homogeneous and isotropic porous background permeated by a set of parallel planar fractures. The background consists of a single isotropic elastic grain material with bulk modulus K_g. The background has porosity ϕ_p and Lame constants λ and μ, with a stiffness tensor of the form

$$\mathbf{c}_b = \begin{bmatrix} \lambda+2\mu & \lambda & \lambda & 0 & 0 & 0 \\ \lambda & \lambda+2\mu & \lambda & 0 & 0 & 0 \\ \lambda & \lambda & \lambda+2\mu & 0 & 0 & 0 \\ 0 & 0 & 0 & \mu & 0 & 0 \\ 0 & 0 & 0 & 0 & \mu & 0 \\ 0 & 0 & 0 & 0 & 0 & \mu \end{bmatrix}. \tag{1}$$

The set of parallel fractures is described by the linear slip model (Schoenberg and Douma (1988); Schoenberg and Sayers (1995)). In this model, at low frequencies, an elastic medium containing a single set of parallel fractures has the compliance tensor

$$\mathbf{s}^0 = \mathbf{s}_b + \mathbf{s}_c, \tag{2}$$

where $\mathbf{s}_b$ is the compliance tensor (inverse of stiffness tensor $\mathbf{c}_b$) of the background and $\mathbf{s}_c$ is the excess compliance tensor associated with the fractures. In this paper we assume the fracture set is rotationally invariant about the x_1 axis, which is normal to the fracture

plane. The excess compliance tensor can be expressed in the form (Schoenberg and Sayers (1995))

$$\mathbf{s}_c = \begin{bmatrix} Z_N & 0 & 0 & 0 & 0 & 0 \\ 0 & 0 & 0 & 0 & 0 & 0 \\ 0 & 0 & 0 & 0 & 0 & 0 \\ 0 & 0 & 0 & 0 & 0 & 0 \\ 0 & 0 & 0 & 0 & Z_T & 0 \\ 0 & 0 & 0 & 0 & 0 & Z_T \end{bmatrix}, \tag{3}$$

where Z_N and Z_T are the normal and tangential excess compliances that exist due to the presence of the fractures.

Stiffness tensor of a fluid-saturated fractured medium – low frequency limit

In his landmark paper, Gassmann (1951) presented equations giving the elastic properties of a fluid saturated anisotropic solid consisting of a single isotropic elastic grain material in the low frequency limit. The relationship between dry and saturated moduli can be written as

$$c_{ij}^{sat} = c_{ij}^0 + \alpha_i \alpha_j M, \qquad i,j = 1,2,...,6 \tag{4}$$

where for transverse isotropy (see Gurevich (2003))

$$\alpha_1 = 1 - \frac{c_{11}^0 + 2c_{13}^0}{3K_g}, \tag{5}$$

$$\alpha_2 = \alpha_3 = 1 - \frac{c_{13}^0 + c_{23}^0 + c_{33}^0}{3K_g} \tag{6}$$

and $\alpha_4 = \alpha_5 = \alpha_6 = 0$. The scalar M is the direct analog of Gassmann's pore space modulus:

$$M = \frac{K_g}{\left(1 - \frac{K^*}{K_g}\right) - \phi\left(1 - \frac{K_g}{K_f}\right)}, \tag{7}$$

where ϕ is the overall porosity of the fractured rock (sum of background porosity ϕ_p and fracture porosity ϕ_c), K_f is the fluid bulk modulus and K^* is the generalized drained bulk

modulus,

$$K^* = \frac{1}{9}\sum_{i=1}^{3}\sum_{j=1}^{3} c_{ij}^0. \tag{8}$$

We can apply these relationships to our dry fractured medium by inverting compliance tensor $\mathbf{s}^0$ to obtain dry stiffnesses c_{ij}^0, which can be substituted into equations 5-8. This yields

$$K^* = K\left(1 - \frac{K}{\lambda + 2\mu}\right)\Delta_N, \tag{9}$$

$$\alpha_1 = 1 - \frac{K}{K_g}\left(1 - \Delta_N\right), \tag{10}$$

$$\alpha_2 = \alpha_3 = \alpha - \frac{K\lambda}{K_g\left(\lambda + 2\mu\right)}\Delta_N, \tag{11}$$

where $K = \lambda + 2\mu/3$ is the bulk modulus of the dry host rock, $\alpha = 1 - K/K_g$ is the Biot-Willis coefficient (Biot and Willis (1957)) and

$$\Delta_N = \frac{(\lambda + 2\mu)Z_N}{1 + (\lambda + 2\mu)Z_N}, \tag{12}$$

$$\Delta_T = \frac{\mu Z_T}{1 + \mu Z_T} \tag{13}$$

denote dimensionless fracture weaknesses.

Stiffness tensor of a fluid-saturated fractured medium – high frequency limit

The results of the previous section assume hydraulic equilibrium between the pore space and fractures, hence are only valid in the low frequency limit. This regime is called "relaxed" by Mavko and Jizba (1991), and corresponds to the situation where the fluid diffusion length (Hudson et al. (2001))

$$J = \sqrt{\phi_p K_f \kappa / 2\eta\omega} \tag{14}$$

is larger than the fracture size (a) and fracture thickness (c),

$$c \ll a \ll J \tag{15}$$

where ω is frequency, κ the background permeability and η the dynamic fluid viscosity. At higher frequencies fluid will not have sufficient time to flow between pore space and fractures. This occurs when the fracture opening becomes larger than the fluid diffusion length (Norris (1993); Gurevich and Lopatnikov (1995); Hudson et al. (2001)), although fractures are still assumed to be smaller than the wavelength. This regime is called "unrelaxed" by Mavko and Jizba (1991). In this regime flow between pores and fractures may be ignored, and the fractures can be treated as isolated fractures in an isotropic background whose stiffness tensor $\mathbf{c}_b^{sat}$ is given by the isotropic Gassmann equation with saturated moduli $L_{sat} = \lambda + 2\mu + \alpha^2 M$ and $\lambda_{sat} = \lambda + \alpha^2 M$. The compliance matrix at high frequencies will then have the form

$$\mathbf{s}^0 = \mathbf{s}_b^{sat} + \mathbf{s}_c^{hf}, \tag{16}$$

where $\mathbf{s}_b^{sat}$ is the inverse of stiffness tensor $\mathbf{c}_b^{sat}$ and $\mathbf{s}_c^{hf}$ is the excess compliance due to fracturing at high frequencies, which we now determine from the results for an isolated crack of radius a and thickness $2c \ll a$. The excess compliances for a crack filled with a weak solid with bulk modulus $K^{'}$ and shear modulus $\mu^{'}$ are (see Schoenberg and Douma (1988); Bakulin, Grechka and Tsvankin (2000))

$$Z_N = \frac{4\epsilon}{3\mu(1-g)\left[1 + \frac{1}{\pi g(1-g)}\left(\frac{K^{'}+4/3\mu^{'}}{\mu}\right)\left(\frac{a}{c}\right)\right]}, \tag{17}$$

$$Z_T = \frac{16\epsilon}{3\mu(3-2g)\left[1 + \frac{4}{\pi(3-2g)}\left(\frac{\mu^{'}}{\mu}\right)\left(\frac{a}{c}\right)\right]}, \tag{18}$$

where $\epsilon = n_0 a^3 = (3/4\pi)(a/c)\phi_c$ is the crack density (Hudson, 1980), $\phi_c = (4/3)\pi a^2 c n_0$ is the additional porosity present due to the cracks, $g = \mu/L$ and n_0 is the number of cracks per unit volume. For fluid-filled cracks, $\mu^{'} \to 0$, however $K^{'}$ for a fluid such as water or oil may be comparable in magnitude to μ. So for thin cracks with small aspect ratio c/a, $\left[\left(K^{'} + 4/3\mu^{'}\right)/\mu\right](a/c) \gg 1$ causing Z_N to go to zero. Z_T, however, remains the same as for dry cracks. Thus the high-frequency excess compliance tensor can be computed by putting Z_N to zero while keeping Z_T the same as for the dry medium in the excess

compliance matrix:

$$\mathbf{s}_c^{hf} = \begin{bmatrix} 0 & 0 & 0 & 0 & 0 & 0 \\ 0 & 0 & 0 & 0 & 0 & 0 \\ 0 & 0 & 0 & 0 & 0 & 0 \\ 0 & 0 & 0 & 0 & 0 & 0 \\ 0 & 0 & 0 & 0 & Z_T & 0 \\ 0 & 0 & 0 & 0 & 0 & Z_T \end{bmatrix}. \tag{19}$$

Frequency dependent wave propagation normal to fractures

Fractures whose size is much smaller than their spacing can be modeled as penny-shaped cracks. This leads to the problem of the interaction of a plane longitudinal elastic wave with an open oblate spheroidal crack of radius a and thickness $2c \ll a$ placed perpendicular to the direction of wave propagation. This problem was considered by Galvin and Gurevich (2007) who investigated the case of so-called mesoscopic cracks whose radius is small compared to the wavelength of the normal compressional wave, but large compared to the individual pore size. Furthermore crack thickness (but not crack radius!) was assumed smaller than the fluid diffusion length. The aspect ratio is assumed to be small, the precise condition being $c/a \ll K_f/\mu$. As shown by Gurevich and Lopatnikov (1995) and Müller and Gurevich (2005), the interaction of propagating waves in heterogeneous poroelastic media and the resulting attenuation can be treated as a scattering problem from fast into slow P-waves, which can be mathematically posed as a mixed boundary value problem for Biot's equations of poroelasticity with boundary conditions. It was also assumed that the crack is in hydraulic communication with the host rock. Together with the small thickness assumption this allows one to neglect the volume change of the crack-filling fluid. As a consequence, the sum of total and relative displacement normal to the crack surface equals zero, in addition to standard conditions of the continuity of total stress and pore pressure, while outside of the crack bulk and relative fluid displacements are assumed continuous. Using these boundary conditions and making use of the cylindrical crack symmetry, the scattering problem can be transformed into a single integral equation (Fredholm equation of the second kind) in

an unknown wave-amplitude function (Galvin and Gurevich, 2007). This single scattering solution can be used to estimate attenuation and dispersion of an elastic wave propagating in a medium with a random distribution of aligned cracks using multiple scattering theory. A Foldy-type approximation of multiple scattering (Waterman and Truell, 1961) can be used to express the effective wavenumber for the medium with cracks in terms of the number of scatterers per unit volume and the far-field forward scattering amplitude for a single scatterer, (Galvin and Gurevich, 2006).

The theory presented by Galvin and Gurevich (2006) gives simple expressions for the low- and high-frequency asymptotic behaviour of velocity and attenuation, but at intermediate frequencies requires numerical solution of an integral equation. In the low-frequency limit, the effective saturated P-wave modulus reads

$$\frac{1}{C_0} = \frac{1}{C}\left[1 + \frac{2\epsilon\left(C - \alpha M\right)^2}{3\mu C(1-g)}\right] \tag{20}$$

where C is the saturated P-wave modulus in the background. Low and high-frequency asymptotes are (Galvin and Gurevich, 2006):

$$\frac{1}{c_{11}^{sat}(\omega)} = \frac{1}{C_0}\left[1 + \frac{i\omega}{D}\frac{2M\left(C - \alpha M\right)^2\left(2 - 4\alpha g + 3\alpha^2 g^2\right)a^2\epsilon}{15\mu g(1-g)^2 C^2}\right] \tag{21}$$

for $\omega \ll \omega_c$ and

$$\frac{1}{c_{11}^{sat}(\omega)} = \frac{1}{C}\left[1 + \frac{2\sqrt{D}\pi\epsilon\left(C - \alpha M\right)^2}{LM\sqrt{-i\omega}a}\right] \tag{22}$$

for $\omega \gg \omega_c$, respectively, where ω is angular frequency, $D = ML\kappa/\eta C$ is the hydraulic diffusivity of the background medium, η is fluid viscosity, κ is intrinsic permeability and $\omega_c = 4\pi D/a^2$ is the crossover frequency of this attenuation mechanism, where the fluid diffusion length is of the order of the crack radius a.

Results for the attenuation and velocity as a function of frequency from this theory can only be obtained numerically (by solving an integral equation) which presents a certain inconvenience of analysis. We can obtain an analytical approximation to the exact numerical solution using the branching function approximation of Johnson (2001). This

branching function accurately approximates the governing frequency dependent complex modulus of the porous medium given the known low- and high-frequency asymptotes of the exact solution, and obeys conditions of causality and non-negative dissipation:

$$\frac{1}{c_{11}^{sat}(\omega)} = \frac{1}{C}\left[1 + \left(\frac{C - C_0}{C_0}\right) / \left(1 - \varsigma + \varsigma\sqrt{1 - \frac{i\omega\tau}{\varsigma^2}}\right)\right] \tag{23}$$

where the P-wave moduli of the fractured and host (unfractured) rock $C_0 \equiv c_{11}^{sat}(0)$ and $C = K^{sat} + 4\mu/3$ are low and high frequency limits of the P-wave modulus, respectively. The behaviour of the attenuation and dispersion in equation (23) is controlled by two parameters: $\varsigma \geq 0$ and $\tau > 0$. Parameter ς controls the shape of the attenuation and dispersion curves while τ defines the time scaling. The time scaling and shape parameters are related to the low- and high-frequency scaling coefficients by

$$\tau = \left(\frac{C - C_0}{CG}\right)^2, \qquad \varsigma = \frac{(C - C_0)^3}{2C_0C^2TG^2}, \tag{24}$$

where the parameters T and G are obtained from asymptotic expressions (21) and (22), respectively:

$$T = \frac{2\left(C - \alpha M\right)^2\left(2 - 4\alpha g + 3\alpha^2 g^2\right)\eta a^2\epsilon}{15\mu g(1-g)^2C^2} \tag{25}$$

and

$$G = 2\pi\epsilon\left(C - \alpha M\right)^2\sqrt{\frac{\kappa}{\eta CML}}. \tag{26}$$

FULL STIFFNESS TENSOR

The stiffness tensor for the entire frequency range is calculated from the low- and high-frequency limits using the branching function of Johnson (2001). Specifically, we calculate each component of the frequency dependent stiffness tensor using an equation analogous to equation (23):

$$\frac{1}{c_{ij}^{sat}(\omega)} = \frac{1}{c_{ij,hf}^{sat}}\left[1 + \left(\frac{c_{ij,hf}^{sat} - c_{ij,lf}^{sat}}{c_{ij,lf}^{sat}}\right) / \left(1 - \varsigma + \varsigma\sqrt{1 - \frac{i\omega\tau}{\varsigma^2}}\right)\right], \tag{27}$$

where $c^{sat}_{ij,hf}$ and $c^{sat}_{ij,lf}$ are the stiffness tensors in the high and low frequency limits and τ and ς are given by equation (24). This interpolation assumes that both the shape and characteristic frequency (but not the magnitude!) of the dispersion remain the same for all directions of propagation. This assumption is justified by the fact that for aligned fractures, the wave-induced flow of the fluid, i.e the slow wave, between fractures and pores is always normal to the fractures due to its low velocity. This assumption is also supported by numerical simulations (Lambert, Gurevich and Brajanovski (2005); Krzikalla and Müller (2011)). Once the complex and frequency-dependent stiffness tensor is known, it can be used to compute complex velocities of quasi-P, SV and SH waves as functions of angle and frequency using the same formulas as used for elastic media (Mavko, Mukerji and Dvorkin (1998), section 2.2)

$$V_P = (c_{11}\sin^2\theta + c_{33}\cos^2\theta + c_{44} + \sqrt{N})^{1/2}(2\rho)^{-1/2}, \tag{28}$$

$$V_{SV} = (c_{11}\sin^2\theta + c_{33}\cos^2\theta + c_{44} - \sqrt{N})^{1/2}(2\rho)^{-1/2}, \tag{29}$$

$$V_{SH} = \left(\frac{c_{66}\sin^2\theta + c_{44}\cos^2\theta}{\rho}\right)^{1/2}. \tag{30}$$

Symbols SV and SH refer to S-waves polarised in the plane normal to fractures and parallel to the fractures, respectively. Then the phase velocities can be computed as (see Carcione et al. (2013))

$$v_p = \left[\mathrm{Re}\left(\frac{1}{v}\right)\right]^{-1}, \tag{31}$$

where v is the velocity of either a qP, qSV or SV wave. The ratio of real to imaginary part of the stiffness gives the anisotropic attenuation matrix $Q_{ij} = \mathrm{Re}(c^{sat}_{ij})/\,\mathrm{Im}(c^{sat}_{ij})$ (Carcione (2007); Zhu and Tsvankin (2006)). The phase attenuation along a given direction can be computed as the ratio of imaginary to real part of the corresponding complex phase slowness (inverse of the complex velocity). We can then compute Thomsen (1986) anisotropy parameters from the real part of the stiffnesses, and attenuation anisotropy parameters using

the notation introduced by Zhu and Tsvankin (2006):

$$\epsilon_Q = \frac{Q_{33} - Q_{11}}{Q_{11}}, \tag{32}$$

$$\delta_Q = \frac{\left(\frac{1}{Q_{13}} + \frac{1}{Q_{55}}\right)^2 - \left(\frac{1}{Q_{33}} - \frac{1}{Q_{55}}\right)^2}{\frac{2}{Q_{33}}\left(\frac{1}{Q_{33}} - \frac{1}{Q_{55}}\right)}. \tag{33}$$

RESULTS

Numerical illustrations are calculated for a fluid-saturated fractured porous rock with the following properties: Poisson's ratio of $\nu = 0.15$, $K_f = 2.25 \times 10^9$ Pa, $K_g = 37 \times 10^9$ Pa, $\mu_g = 44 \times 10^9$ Pa, $\phi = 0.3$, $\epsilon = 0.1$, $\eta = 10^{-3}$ Pa.s, $\kappa = 1$ D, and densities of $\rho_f = 1000$ kg$\times$m^{-3} and $\rho_g = 2650$ kg$\times$m^{-3}. Figure 2 shows dispersion of P waves for different angles to the fracture symmetry axis. Figure 3 shows dispersion of the SV wave at an angle of 45°.The SH wave is not shown as it is not dispersive, and has a constant velocity of around 1407 m$\times$s^{-1}. As expected the greatest dispersion occurs normal to the fractures, when the coupling between the incident wave and slow wave is at it's maximum. Figure 4 shows the corresponding attenuation curves for different angles of incidence, attenuation also being largest for propagation normal to fractures. Another way to express these results is by plotting as a function of incident angle, for three representative frequencies: low (10^{-2} Hz), intermediate (10^3 Hz), and high (10^8 Hz). Figure 5 shows variation of P wave velocity with angle of incidence for low, intermediate and high frequencies. Velocities decrease as propagation becomes normal to fractures. Figure 6 shows variation of SV wave velocity with angle of incidence for low, intermediate and high frequencies. The greatest variation is at 45° to the fractures. Figure 7 shows variation of P wave attenuation with angle of incidence for low, intermediate and high frequencies. Attenuation is greatest for propagation normal to fractures, and peaks between the low and high frequency limits. Figure 8 shows variation of SV wave attenuation with angle of incidence for low, intermediate and high frequencies. Attenuation is greatest for propagation at 45° to the fractures, and peaks between the low and high frequency limits.

A more concise and apparent representation of the frequency dependent anisotropy can be given by computing the frequency dependence of Thomsen's anisotropy parameters. This is shown in Figure 9. We see that at low frequencies, anisotropy parameters ϵ and δ are of the same order of magnitude and thus the medium is close to elliptical. However, as frequency increases, δ changes from positive to negative, while ϵ approaches zero, giving a strongly unelliptical pattern. Figure 10 shows Thomsen-style anisotropy parameters with respect to the vertical axis $\epsilon^{(V)}$ and $\delta^{(V)}$, which are useful for modeling the surface seismic response (assuming that fractures are vertical). The behaviour of the anisotropy parameters can be explained as follows. At low frequencies the behaviour is consistent with anisotropic Gassmann theory, and the stiffness components have values that are equal to the stiffnesses of the dry fractured medium plus a second-order term related to the fluid (as in our example the fluid modulus is small compared to the dry stiffnesses). However at high frequencies, as discussed earlier in the paper, the normal stiffnesses vanishes, and therefore velocities perpendicular and parallel to fractures become equal, and hence ϵ approaches zero. At the same time, at intermediate angles, the velocity is smaller than in the symmetry directions because of the coupling with the SV wave (note that the shear stiffness does not vanish, and thus the medium is still anisotropic). Thus δ does not vanish and serves as the only indicator of P–SV anisotropy. This behaviour of velocities as functions of angle is illustrated in Figures 5-6.

Figure 11 shows the frequency dependence of the attenuation anisotropy parameters of Zhu and Tsvankin (2006), ϵ_Q and δ_Q. This again shows that attenuation anisotropy varies with frequency but this variation expressed through ϵ_Q and δ_Q is not dramatic, and the parameters remain finite (and quite large) even in the limits of low and high frequencies, where attenuation tends to zero. However, the values of the parameters ϵ_Q and δ_Q do have physical meaning: they are related to the relationships between attenuation in different directions as shown in Figure 7. Note that attenuation anisotropy parameters are not small and thus a weak attenuation anisotropy approximation is not applicable. An alternative way to quantify the magnitude of attenuation is to use a dimensionless parameter $\epsilon_{Qa} = 1/Q_{33} - 1/Q_{11}$. This parameter is plotted in Figure 12. This parameter goes to zero

in the low and high frequency limits and has a maximum corresponding to a frequency such that the fluid diffusion length is the same order of magnitude as the crack radius.

DISCUSSION AND CONCLUSIONS

We have proposed a simple model for calculating the complex and frequency dependent stiffness tensor and anisotropic attenuation of a porous rock with a single set of aligned fractures. By construction, the model is consistent with known results for the stiffness tensor of a fractured porous medium in the low and high frequency limits and allows one to compute phase velocities and attenuation factors for quasi P, SV and SH waves as functions of frequency and angle. The behaviour of P and SV waves as a function of frequency and angle is consistent in the low and high frequency limits with the fact that attenuation and dispersion in this medium is due to conversion from P and SV waves into the Biot slow wave, diffusion of crack-filling fluid between the crack and surrounding background porosity. Velocity and attenuation anisotropy parameters have also been calculated and exhibit the important results in a concise fashion. It is interesting to note that while at low frequencies the medium is close to elliptical (which is to be expected as a dry medium containing a distribution of penny-shaped cracks is known to be close to elliptical), at high frequencies the coupling between P and SV waves results in anisotropy due to the non-vanishing excess tangential compliance Z_T.

The approach introduced in this paper is very similar to the one proposed by Carcione et al. (2013). The main differences are related to the underlying fracture models: the work of Carcione et al. (2013) is based on the model of infinite planar fractures (Brajanovski et al. (2005)), while our work is based on the model of penny-shaped fractures in a poroelastic background (Galvin and Gurevich (2009)). Comparison of these models for wave propagation normal to fractures shows that they have similar results at high frequencies, but differ in attenuation asymptotics at low frequencies (Gurevich et al. (2009)). Since in both approaches all the stiffness components are derived from the frequency dependence at normal incidence, these differences in the frequency dependency of attenuation are also present for other directions of wave propagation. Furthermore, both the model of Carcione et al.

(2013) and the present work are consistent with the anisotropic Gassmann equations in the low frequency limit, and with the isolated crack model in the high frequency limit, the behaviour of velocities and elastic anisotropy parameters in these limits is the same in both models.

We conclude that the simple methodology presented here for approximating the frequency dependent stiffness tensor of a fractured fluid-saturated porous medium should be useful in describing the variation of wave velocities in different directions and at varying frequencies.

REFERENCES

Bakulin, A., V. Grechka, and I. Tsvankin, 2000, Estimation of fracture parameters from reflection seismic data – Part I: HTI model due to a single fracture set: Geophysics, **65**, 1788–1802.

Behura, J., and I. Tsvankin, 2009, Estimation of interval anisotropic attenuation from reflection data: Geophysics, **74**, A69–A74.

Best, A. I., J. Sothcott, and C. McCann, 2007, A laboratory study of seismic velocity and attenuation anisotropy in near-surface sedimentary rocks: Geophysical Prospecting, **55**, 609–625.

Biot, M. A., 1962, Mechanics of deformation and acoustic propagation in porous media: J. Appl. Phys., **33**, 1482–1498.

Biot, M. A., and D. G. Willis, 1957, The elastic coefficients of the theory of consolidation: J. App. Mech., **24**, 594–601.

Brajanovski, M., B. Gurevich, and M. Schoenberg, 2005, A model for P-wave attenuation and dispersion in a porous medium permeated by aligned fractures: Geophys. J. Internat., **163**, 372–384.

Brown, L., and B. Gurevich, 2004, Frequency-dependent seismic anisotropy of porous rocks with penny-shaped cracks: Exploration Geophysics, **35(2)**, 111–115.

Brown, R. J. S., and J. Korringa, 1975, On the dependence of the elastic properties of a porous rock on the compressibility of the pore fluid: Geophysics, **40**, 608–616.

Carcione, J. M., 2007, Theory and numerical simulation of wave propagation in anisotropic, anelastic, porous and electromagnetic media: Elsevier.

Carcione, J. M., B. Gurevich, J. E. Santos, and S. Picotti, 2013, Angular and frequency-dependent wave velocity and attenuation in fractured porous media: Pure Appl. Geophys., **170**, 1673–1683.

Carcione, J. M., S. Picotti, and J. E. Santos, 2012a, Numerical experiments of fracture-induced velocity and attenuation anisotropy: Geophys. J. Internat., **191**, 1179–1191.

Carcione, J. M., J. E. Santos, and S. Picotti, 2012b, Fracture-induced anisotropic attenuation: Rock Mechanics and Rock Engineering, **45**, 929–942.

Cardona, R., 2002, Two theories for fluid substitution in porous rocks with aligned cracks: 72st Ann. Internat. Mtg., Soc. Expl. Geophys., Expanded Abstracts, 173–176.

Chapman, M., 2003, Frequency dependent anisotropy due to meso-scale fractures in the presence of equant porosity: Geophys. Prosp., **51**, 369–379.

Chichinina, T. I., I. R. Obolentseva, L. Gik, B. Bobrov, and G. Ronquillo-Jarillo, 2009a, Attenuation anisotropy in the linear-slip model: Interpretation of physical modeling data: Geophysics, **74**, WB165–WB176.

Chichinina, T. I., I. R. Obolentseva, and G. Ronquillo-Jarillo, 2009b, Anisotropy of seismic attenuation in fractured media: theory and ultrasonic experiment: Transport in Porous Media, **79**, 1–14.

Clark, R. A., P. M. Benson, A. J. Carter, and C. A. Guerrero-Moreno, 2009, Anisotropic p-wave attenuation measured from a multi-azimuth surface seismic reflection survey: Geophysical Prospecting, **57**, 835–845.

Galvin, R. J., and B. Gurevich, 2006, Interaction of an elastic wave with a circular crack in a fluid-saturated porous medium: Appl. Phys. Lett., **88**, 061918.

———, 2007, Scattering of a longitudinal wave by a circular crack in a fluid-saturated porous medium: International Journal of Solids and Structures, **44**, 7389–7398.

———, 2009, Effective properties of a poroelastic medium containing a distribution of aligned cracks: J. Geophys. Res., **114**, B07305.

Gassmann, F., 1951, Über die elastizität poröser medien: Viertel. Naturforsch. Ges. Zürich, **96**, 1–23.

Gurevich, B., 2003, Elastic properties of saturated porous rocks with aligned fractures: Journal of Applied Geophysics, **54**, 203–218.

Gurevich, B., M. Brajanovski, R. Galvin, T. Muller, and J. Toms-Stewart, 2009, P-wave dispersion and attenuation in fractured and porous reservoirs - poroelasticity approach: Geophysical Prospecting, **57**, 225–237.

Gurevich, B., and S. L. Lopatnikov, 1995, Velocity and attenuation of elastic waves in finely layered porous rocks: Geophys. J. Internat., **121**, 933–947.

Hudson, J., T. Pointer, and E. Liu, 2001, Effective-medium theories for fluid-saturated materials with aligned cracks: Geophys. Prosp., **49**, 509–522.

Hudson, J. A., 1980, Overall properties of a cracked solid.: Math. Proc. Camb. Phil. Soc., **88**, 371–384.

Hudson, J. A., E. Liu, and S. Crampin, 1996, The mechanical properties of materials with interconnected cracks and pores.: Geophys. J. Internat., **124**, 105–112.

Jakobsen, M., T. A. Johansen, and C. McCann, 2003, The acoustic signature of fluid flow in complex porous media: Journal of Applied Geophysics, **54**, 219–246.

Johnson, D. L., 2001, Theory of frequency dependent acoustics in patchy-saturated porous media: J. Acoust. Soc. Amer., **110**, 682–694.

Krzikalla, F., and T. Müller, 2011, Anisotropic p-sv-wave dispersion and attenuation due to inter-layer flow in thinly layered porous rocks: Geophysics, **76**, WA135–WA145.

Lambert, G., B. Gurevich, and M. Brajanovski, 2005, Frequency dependent anisotropy of porous fractured rocks: Presented at the 67th EAGE Conference and Exhibition,Madrid, Expanded Abstracts.

Maultzsch, S., M. Chapman, E. Liu, and X. Li, 2003, Modelling frequency-dependent seismic anisotropy in fluid-saturated rock with aligned fractures: implication of fracture size estimation from anisotropic measurements: Geophysical Prospecting, **51**, 381–392.

Mavko, G., and D. Jizba, 1991, Estimating grain-scale fluid effects on velocity dispersion in rocks: Geophysics, **56**, 1940–1949.

Mavko, G., T. Mukerji, and J. Dvorkin, 1998, The rock physics handbook: Tools for seismic analysis in porous media: Cambridge University Press.

Müller, T., and B. Gurevich, 2005, Wave-induced fluid flow in random porous media: Attenuation and dispersion of elastic waves: J. Acoust. Soc. Amer., **117**, 2732–2741.

Norris, A. N., 1993, Low-frequency dispersion and attenuation in partially saturated rocks: J. Acoust. Soc. Amer., **94**, 359–370.

Schoenberg, M., and J. Douma, 1988, Elastic-wave propagation in media with parallel fractures and aligned cracks: Geophys. Prosp., **36**, 571–590.

Schoenberg, M., and C. M. Sayers, 1995, Seismic anisotropy of fractured rock: Geophysics, **60**, 204–211.

Thomsen, L., 1986, Weak elastic anisotropy: Geophysics, **51**, 1954–1966.

———, 1995, Elastic anisotropy due to aligned cracks in porous rock: Geophysical Prospect-

ing, **43**, 805–829.

Waterman, P. C., and R. Truell, 1961, Multiple scattering of waves: J. Math. Phys., **2**, 512–537.

Wenzlau, F., J. B. Altmann, and T. Müller, 2010, Anisotropic dispersion and attenuation due to wave-induced fluid flow: Quasi-static finite element modeling in poroelastic solids: J. Geophys. Res., **115**, B07204.

Zhu, Y., and I. Tsvankin, 2006, Plane-wave propagation in attenuative transversely isotropic media: Geophysics, **71**, T17–T30.

Zhu, Y., I. Tsvankin, and K. van Wijk, 2007, Physical modelling and analysis of p-wave attenuation anisotropy in transversely isotropic media: Geophysics, **72**, D1–D7.

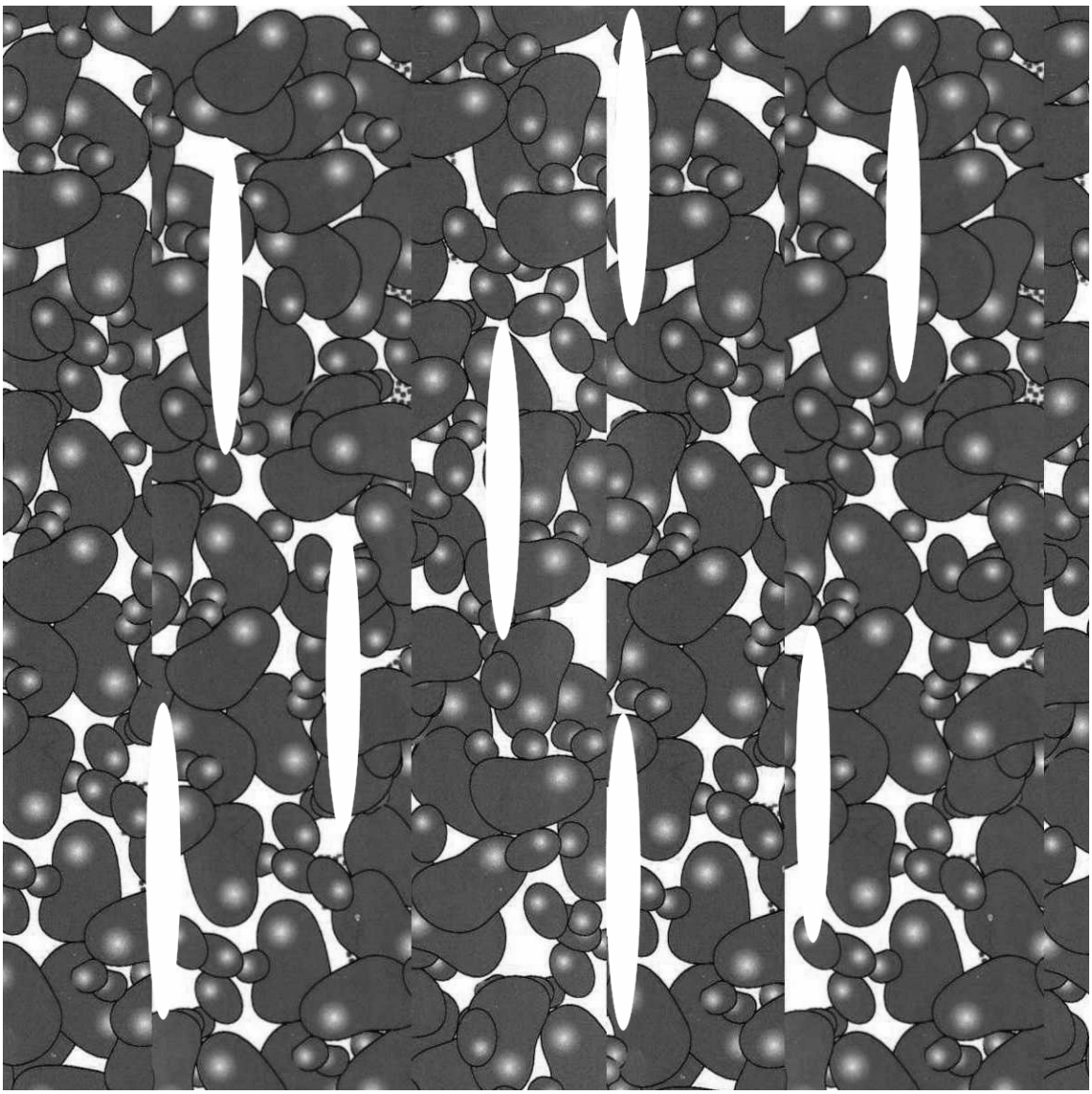

Figure 1: A porous medium containing a sparse distribution of circular cracks.

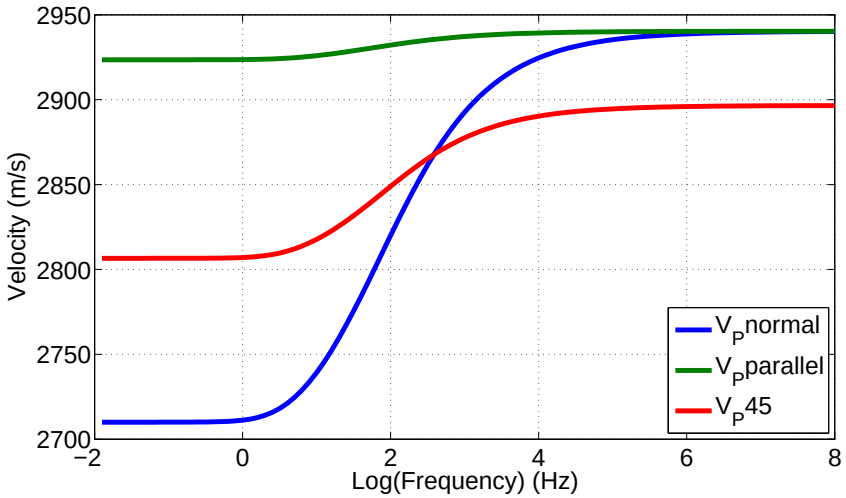

Figure 2: Frequency dependency of P wave phase velocity for different angles to the fracture symmetry axis.

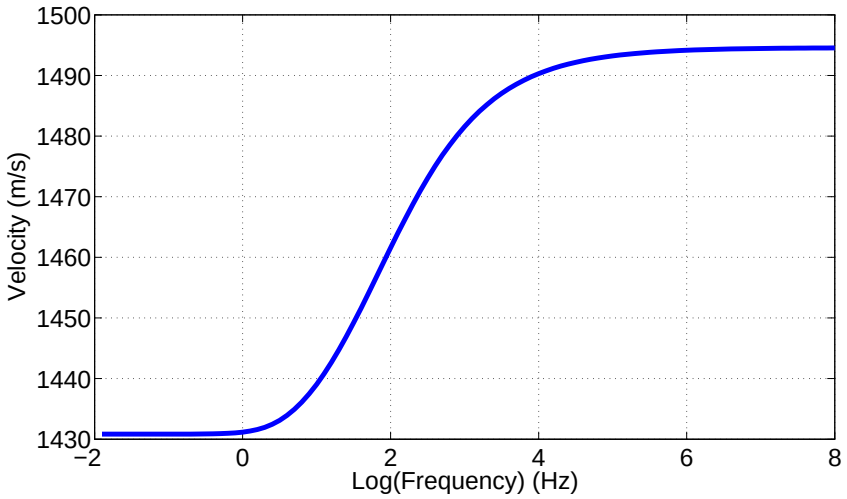

Figure 3: Frequency dependency of SV wave phase velocity at 45 degrees to the fracture symmetry axis.

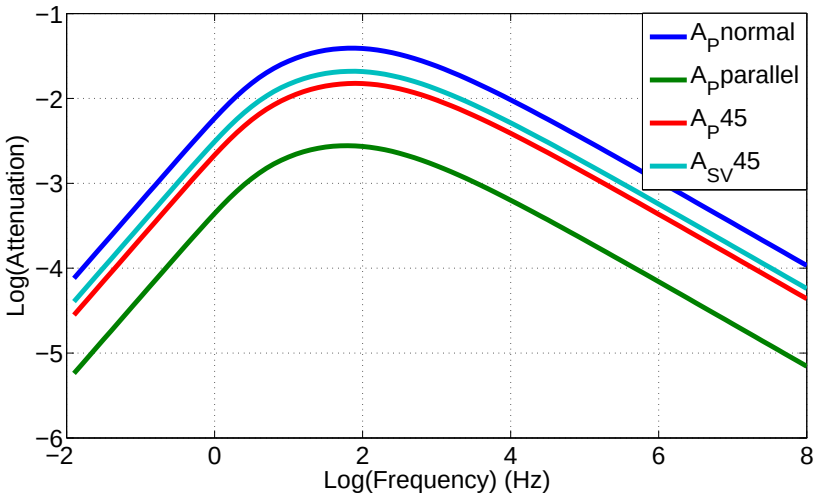

Figure 4: Attenuation of P and SV waves for different angles to the fracture symmetry axis.

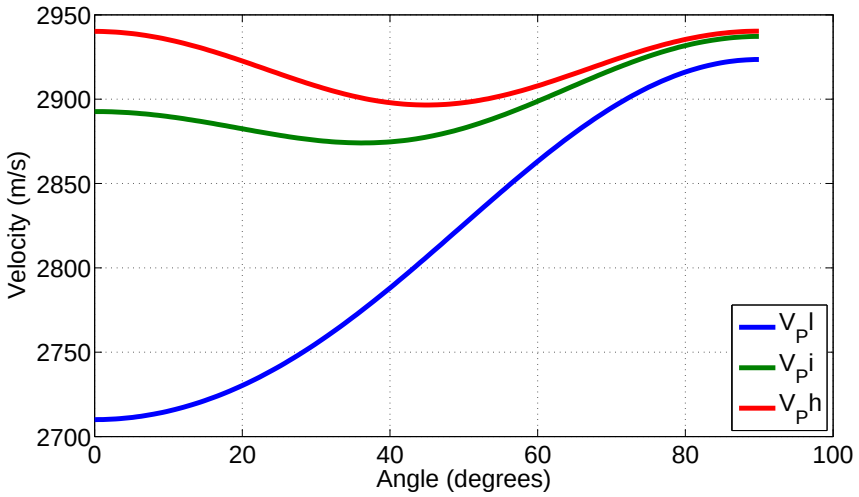

Figure 5: Variation of P wave velocity with angle of incidence for low, intermediate and high frequencies.

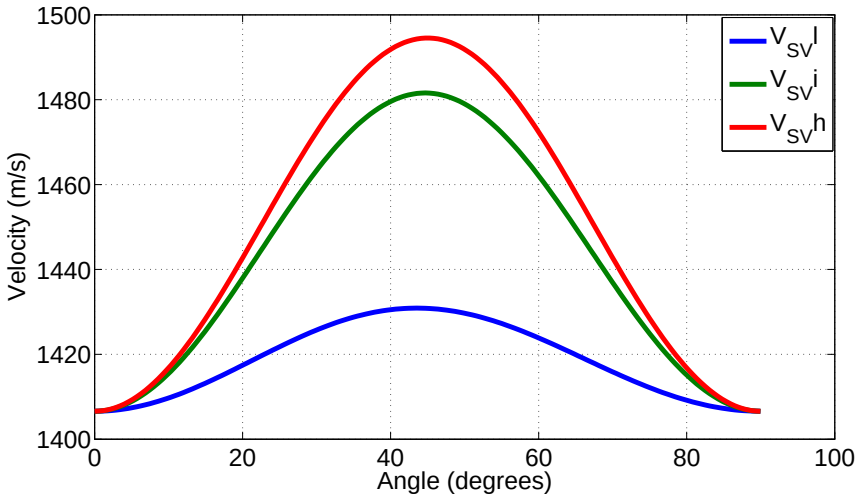

Figure 6: Variation of SV wave velocity with angle of incidence for low, intermediate and high frequencies.

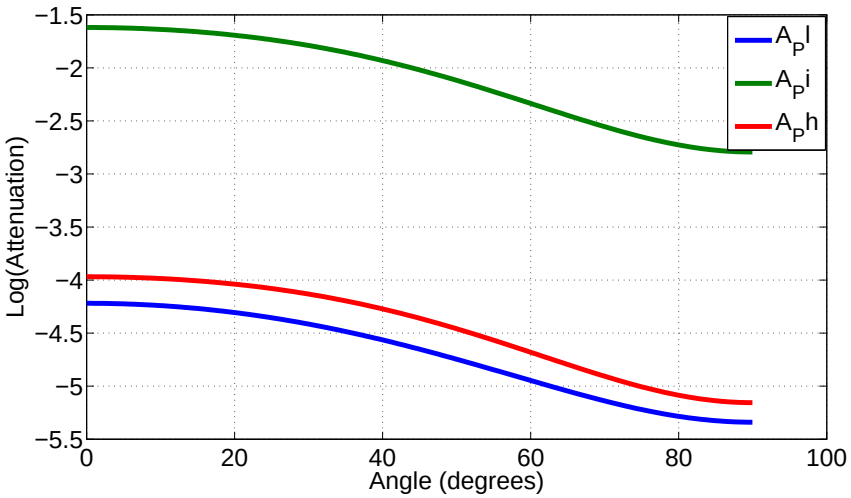

Figure 7: Variation of P wave attenuation with angle of incidence for low, intermediate and high frequencies.

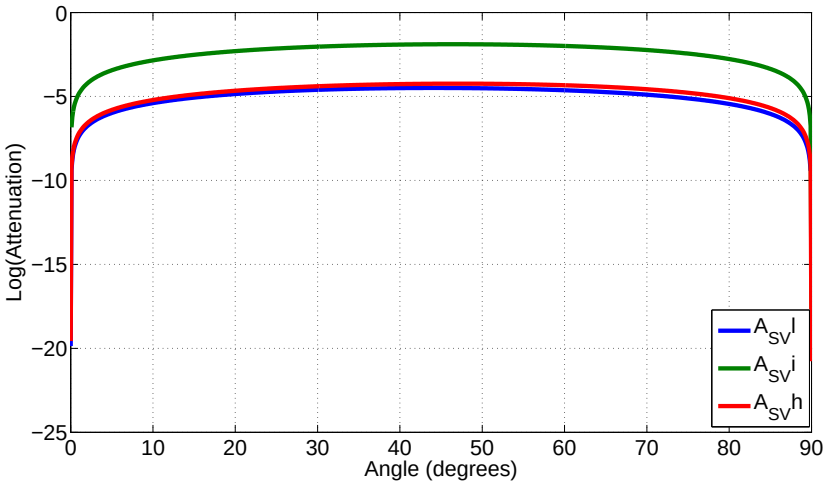

Figure 8: Variation of SV wave attenuation with angle of incidence for low, intermediate and high frequencies.

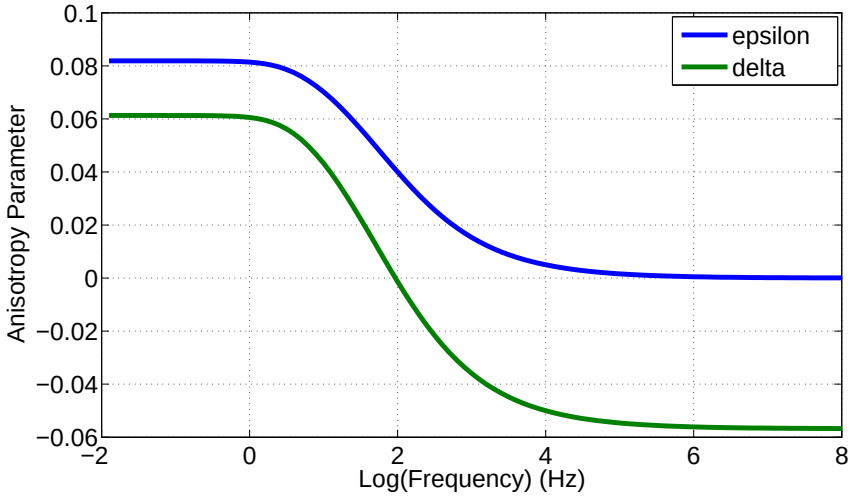

Figure 9: Frequency dependence of Thomsen's anisotropy parameters for horizontal symmetry axis.

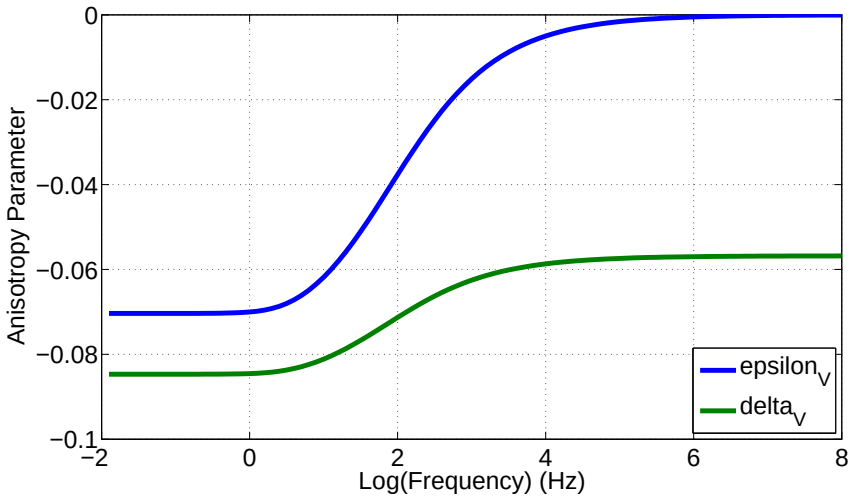

Figure 10: Frequency dependence of Thomsen's anisotropy parameters for vertical symmetry axis.

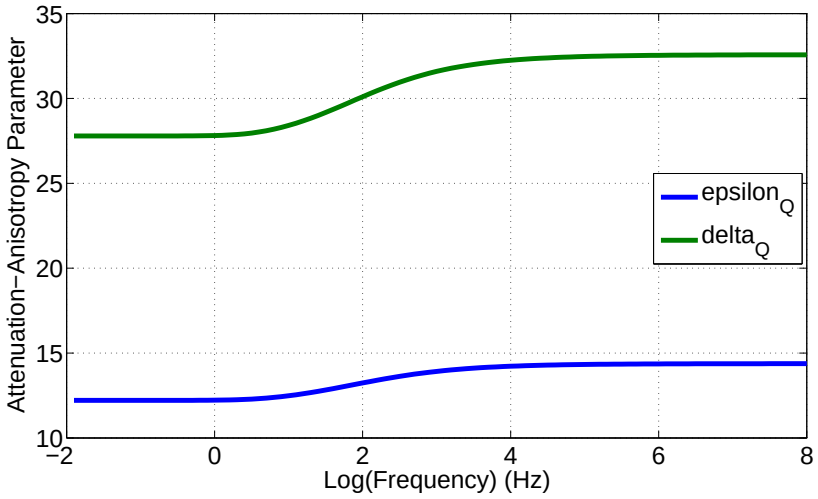

Figure 11: Frequency dependence of attenuation anisotropy parameters.

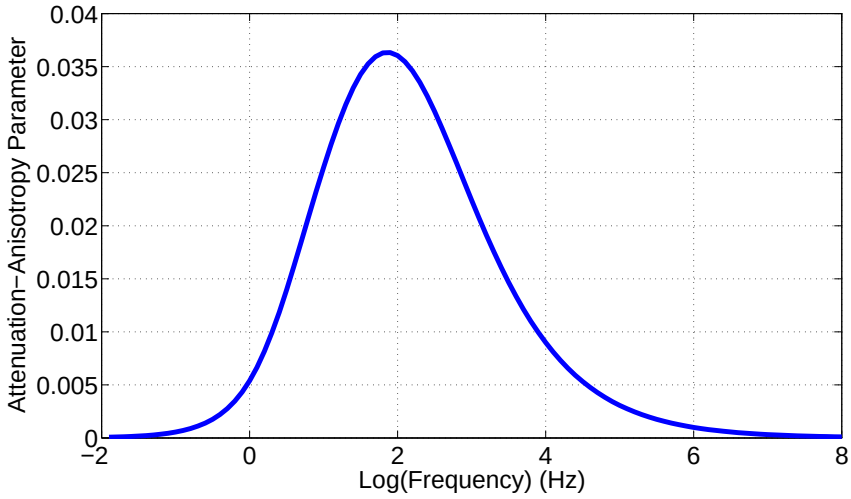

Figure 12: Frequency dependence of alternative attenuation anisotropy parameter epsilonQ.